PHYSICAL REVIEW A **84**, 061805(R) (2011)

# Preparation of subradiant states using local qubit control in circuit QED

S. Filipp,* A. F. van Loo, M. Baur, L. Steffen, and A. Wallraff
*Department of Physics, ETH Zurich, CH-8093 Zurich, Switzerland*
(Received 14 July 2011; published 28 December 2011)

Transitions between quantum states by photon absorption or emission are intimately related to the symmetries of the system which lead to selection rules and the formation of dark states. In a circuit quantum electrodynamics setup, in which two resonant superconducting qubits are coupled through an on-chip cavity and driven via the common cavity field, one single-excitation state remains dark. Here, we demonstrate that this dark state can be excited using local phase control of individual qubit drives to change the symmetry of the excitation field. We observe that the dark state decay via spontaneous emission into the cavity is suppressed, a characteristic signature of subradiance. This local control technique could be used to prepare and study highly correlated quantum states of cavity-coupled qubits.

DOI: 10.1103/PhysRevA.84.061805 PACS number(s): 42.50.Ct, 03.67.Lx, 42.50.Pq, 85.35.Gv

Symmetry properties of a quantum system interacting with a radiation field provide information about possible transitions within the system. Symmetry operations such as translation, rotation, or reflection, which leave the system invariant, lead to selection rules in molecular and solid-state systems [1]. For an ensemble of identical atoms, the symmetry under permutation of particles allows only for transitions between symmetric collective states [2,3]. These highly entangled Dicke states, e.g., the single-excitation W state, have attracted much attention in the field of quantum information processing with trapped ions [4], optical photons [5], and superconducting qubits [6] due to their robustness under decoherence [7] and particle loss [8,9]. Moreover, collective states have been used for quantum information storage in atomic memories [10]. The particular symmetry of Dicke states also affects their decay. Spontaneous emission can be enhanced for superradiant states [2,3], or inhibited, if the symmetry of the state does not allow for the emission of a photon. This effect is known as subradiance and is closely related to the concept of decoherence-free subspaces, regions in Hilbert space which are not affected by decoherence, and therefore are appealing for quantum information processing [11]. Though theoretically well studied [12,13], subradiant states are difficult to realize and experimental evidence of subradiance is rare [14,15].

Here we present a method to prepare two qubits in the antisymmetric Dicke state and demonstrate its subradiance in circuit quantum electrodynamics (QED) [16,17]. In this architecture, superconducting artificial atoms are coupled to a common field mode of a planar microwave cavity. Strong resonant coupling of individual qubits [18–20] and qubit ensembles [21] to single microwave photons has been achieved. Moreover, cavity-mediated interactions between distant qubits [22–24] form the basis for on-chip quantum information processing [25,26] using entangled states of currently up to three qubits [27].

In circuit QED experiments, radiative decay into the cavity—known as the Purcell effect [28]—provides a significant qubit relaxation channel [29]. It can be reduced by operating the individual qubits in the dispersive regime, by advanced circuit designs [30], or by using a tunable coupling qubit that provides Purcell protection within a decoherence-free subspace (DFS) [31,32]. Here, instead, we demonstrate Purcell protection of two cavity-coupled qubits in an antisymmetric superposition state which is prepared using local phase control of the driving microwave field [Fig. 1(a)]. We consider two qubits resonant with each other but not with the cavity, modeled by a generalized Tavis-Cummings Hamiltonian [33],

$$H_{\mathrm{TC}}/\hbar = \omega_r a^\dagger a + \omega_q J_z + g(aJ_+ + a^\dagger J_-), \tag{1}$$

where the dominant cavity mode is at frequency $\omega_r$ and the qubits are at frequency $\omega_q$. The operators $J_z \equiv 1/2\sum_i^N \sigma_z^{(i)}$ and $J_\pm \equiv \sum_i^N \sigma_\pm^{(i)}$ are collective spin operators [3] for $N$ qubits with $\sigma_\pm^{(i)} \equiv (\sigma_x^{(i)} \pm i\sigma_y^{(i)})/2$ and Pauli operators $\sigma_{x,y,z}^{(i)}$ for the individual qubits ($i = 1,2$). $a^{(\dagger)}$ is the annihilation (creation) operator of the field interacting with the qubits with equal coupling strength $g$. For the single-excitation manifold the eigenstates of $H_{\mathrm{TC}}$ are

$$\begin{aligned} |\psi_a\rangle &= |0;\psi_-\rangle, \\ |\psi_r\rangle &= \cos\theta_m|1;gg\rangle + \sin\theta_m|0;\psi_+\rangle, \\ |\psi_s\rangle &= \sin\theta_m|1;gg\rangle - \cos\theta_m|0;\psi_+\rangle, \end{aligned} \tag{2}$$

where the mixing angle $\theta_m$ is given by $\cos 2\theta_m = -\Delta/\sqrt{4(\sqrt{2}g)^2 + \Delta^2}$ with the qubit-resonator detuning $\Delta \equiv \omega_q - \omega_r$. $|n;\rangle$ is a state with $n$ photons in the resonator, and $|\psi_\pm\rangle = (|ge\rangle \pm |eg\rangle)/\sqrt{2}$ are the symmetric and antisymmetric qubit Bell states. Only the qubit state which reflects the symmetry of the cavity mode—i.e., belongs to a compatible irreducible representation of the permutation group [12]—mixes with the field to form the hybridized matter-field states $|\psi_r\rangle$ and $|\psi_s\rangle$. In our case, the coupling to the first harmonic cavity mode has the same sign for both qubits ($g^{(1)} \approx g^{(2)}$) [24]. Therefore, the symmetric qubit state $|\psi_+\rangle$, which is invariant under permutation of the qubits, couples to the photon field [Fig. 1(b)] with enhanced collective coupling strength $\sqrt{N}g$ for $N = 2$ [21]. The antisymmetric qubit state $|\psi_-\rangle$ remains uncoupled and forms the dark state $|\psi_a\rangle$. In general, two hybridized bright states and $(N-1)$ uncoupled dark states are established for an $N$ qubit system.

*filipp@phys.ethz.ch

 

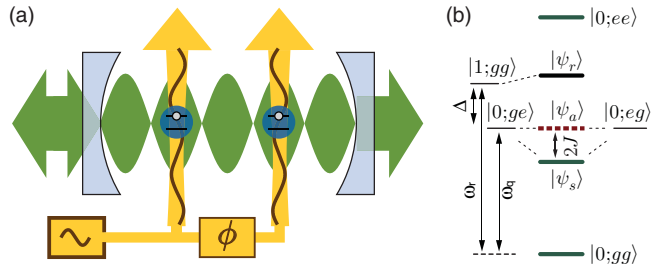


FIG. 1. (Color online) (a) Schematic of a cavity QED setup with individual phase control of the driving field for each qubit. (b) Energy-level diagram of the two-qubit system coupled dispersively to a common cavity field. Symmetric states are indicated by thick solid (green) lines and the antisymmetric state is identified by the thick dashed (red) line.

For our experiments, two superconducting transmon qubits [34] have been integrated into a coplanar niobium resonator on a sapphire substrate [Figs. 2(a) and 2(b)]. The qubits have similar Josephson energies $E_J/h \approx 37.6$ GHz, charging energies $E_C/h \approx 285$ MHz, and coupling strengths $g/2\pi \approx 116$ MHz to the first harmonic mode of the microwave transmission line resonator. The resonator frequency is $\omega_r/2\pi = 6.937$ GHz and its decay rate is $\kappa/2\pi = 3.01$ MHz. In the dispersive regime where $\theta_m \approx \pi$, the photonic contribution $|1;gg\rangle$ to the symmetric state $|\psi_s\rangle$ is small (of order $\sqrt{2}g/\Delta$) and the state has predominantly a qubit character. It is, however, shifted in energy by $2J \equiv 2g^2/\Delta$ corresponding to the dispersive $J$ coupling discussed in Refs. [22] and [24] [Fig. 1(b)]. The antisymmetric wave function $|\psi_a\rangle$ has no photonic component and therefore its energy experiences no Lamb shift. In this description the qubit-qubit coupling $J$ can be understood as the collective Lamb shift $(\sqrt{2}g)^2/\Delta = 2J$ of the symmetric state $|\psi_s\rangle$.

The symmetry of the collective states is also reflected in selection rules for electric dipole transitions. In fact, for a drive applied directly to the cavity, transitions from the ground to the symmetric bright state $|\psi_s\rangle$ are allowed, while transitions to the antisymmetric dark state $|\psi_a\rangle$ are forbidden [24]. The drive conserves the symmetry under permutation of qubits, and only transitions within the class of symmetric states [Fig. 1(b); solid green lines] are allowed [12]. This constraint can be overcome by addressing the qubits individually via capacitively coupled charge lines [35] and tuning the relative phase $\phi$ of the

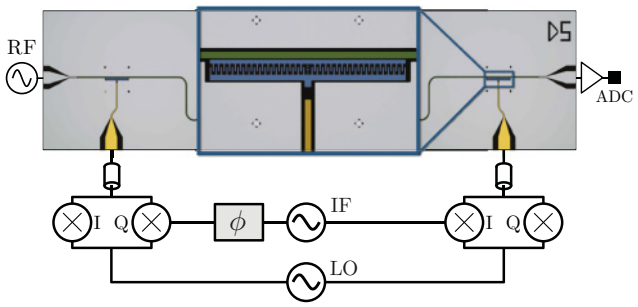


FIG. 2. (Color online) Setup and micrograph of the sample with a transmission line resonator (green) and two transmon qubits (blue) addressable via local charge lines (yellow).

microwave drive at the qubit positions. When choosing a relative phase of $\phi = \pi$, the opposite sign of the local fields results in allowed transitions to the antisymmetric state. This method has been discussed in Ref. [36] and applied recently in flux qubit systems to suppress transitions at degenerate frequencies [37,38].

In the rotating frame, the drive acting on the individual qubits with frequency $\omega_d$ and coupling $\epsilon$ is

$$H_d = \hbar\epsilon(\sigma_+^{(1)} + \xi e^{i\phi}\sigma_+^{(2)}) + \text{H.c.}, \tag{3}$$

where $\xi$ is the amplitude ratio of the local qubit drives. Starting in the ground state, the drive $H_d$ can induce transitions to the state $|\psi\rangle$, if the matrix element $\Omega(\psi) \equiv |\langle\psi|H_d|0;gg\rangle|/\hbar$ is nonzero. The dark state is defined by $\Omega(\psi_{\text{dark}}) = 0$. In the dispersive regime, the matrix element for the symmetric and antisymmetric state is

$$\Omega(\psi_{s/a}) = \epsilon\sqrt{(1 + \xi^2 \pm 2\xi\cos\phi)/2}. \tag{4}$$

$\Omega(\psi_a)$ vanishes for equal drive amplitudes ($\xi = 1$) and zero relative phase ($\phi = 0$), which corresponds to a drive applied to the cavity in the vicinity of the first harmonic mode, and the antisymmetric state $|\psi_a\rangle$ remains dark [24]. For $\phi = \pi$ and $\xi = 1$, however, $\Omega(\psi_a)$ is maximal, while the transition rate $\Omega(\psi_s)$ to the symmetric state vanishes. The transition can thus be enabled or disabled by adjusting the relative phase appropriately.

We have spectroscopically measured the transition amplitude as a function of relative phase $\phi$ between the local qubit drives in the vicinity of the bare qubit frequencies $\omega_q/2\pi = 6.647$ GHz. To control $\phi$, the local microwave fields are generated by a single microwave source operating at the carrier frequency $\omega_{\text{LO}} = \omega_d + \omega_{\text{IF}}$. We use two in-phase & quadrature (IQ) mixers to generate sidebands of the carrier signal at the frequency $\omega_d$. The signal (IF) at the intermediate frequency $\omega_{\text{IF}} = 150$ MHz is synthesized with an arbitrary wave-form generator and applied to each mixer with relative phase $\phi$ [Fig. 2(a)]. The phase $\phi$ of the local qubit drives can then be controlled with high precision by the phase of the IF signals. Pulsed spectroscopy is used [39,40], where the measurement tone is switched on after a 500-ns saturation pulse. The difference between the transmitted signal $s(t)$ and the signal with both qubits in their ground state $s_{gg}(t)$ integrated over $t_m = 520$ ns yields the transmission amplitude $S = \int_0^{t_m}\{s(t) - s_{gg}(t)\}dt$. The measured value of $S$ corresponds to the steady-state population of the single-excited qubit states when appropriately normalized [41]. A signal can also be detected when the qubits are in the antisymmetric state, decoupled from the cavity. The cavity then remains at its bare frequency, in contrast to the frequency shift that is established when both qubits are in the ground state.

Two spectroscopic lines, varying in amplitude as a function of relative phase $\phi$, are observed at $\omega_a/2\pi = 6.647$ GHz and $\omega_s/2\pi = 6.578$ GHz. These correspond to the states $|\psi_a\rangle$ and $|\psi_s\rangle$, respectively. As expected, the zeros of the populations of the symmetric and the antisymmetric state are $\sim 180^\circ$ out of phase (Fig. 3). The measured values are in good agreement with the steady-state population of the excited states calculated using the dissipative Bloch equations for a two-level system driven at zero detuning [42],

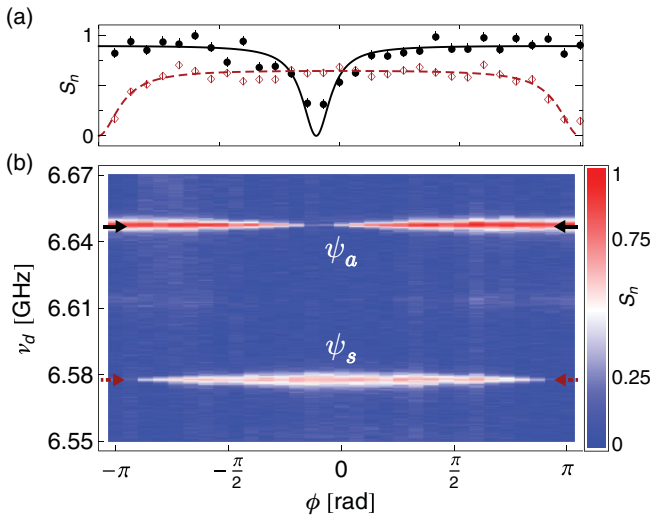


FIG. 3. (Color online) Spectroscopy of dark and bright states as a function of the relative phase $\phi$ between drives. (a) Normalized integrated transmission amplitudes $S_n = S/S_{max}$ of the antisymmetric state $\psi_a$ (black solid dots) and the symmetric state $\psi_s$ (red open diamonds) at the frequencies $\omega_a/2\pi = 6.647$ GHz and $\omega_s/2\pi = 6.578$ GHz, respectively, as indicated by the arrows in (b). $S_n$ is normalized to unity at the maximum value of both curves ($S_{max}$). The lines indicate fits to the expected steady-state populations. (b) Transmission amplitude as a function of frequency $\nu_d$ and relative phase $\phi$ of the spectroscopic saturation pulse.

$S = S_0\{1 - 1/[1 + T_1T_2\Omega(\psi)^2]\}/2$. The scaling factor $S_0$ takes account of the integrated voltage at the analog-digital converter. The dephasing times $T_{2,s} = 322 \pm 26$ ns and $T_{2,a} = 526 \pm 36$ ns of $|\psi_a\rangle$ and $|\psi_s\rangle$ are determined in independent Ramsey-fringe experiments. The energy relaxation times $T_{1,s}$ and $T_{1,a}$ are measured in separate time-delay experiments and are discussed below. From independent fits of $S$ to both curves using $\Omega(\psi_{s/a})$ from Eq. (4), we obtain the relative phase difference $\phi_s - \phi_a = \pi - 0.3 \pm 0.03$ rad between the zeros of the populations of the symmetric and the antisymmetric state. The deviation of the measured phase difference from $\pi$ is simply caused by the difference in cable lengths of the two-qubit drive lines. In addition, we have determined an on-off ratio $\gtrapprox 14$ from Rabi oscillations of the antisymmetric state population driven with a relative phase difference of 0 and $\pi$.

Using the presented method, it is possible to verify the subradiant character of the antisymmetric state by testing its resilience to cavity-induced Purcell decay [28], which is caused by the indirect coupling of the qubits to the environment via the cavity. According to Fermi's golden rule, the induced voltage fluctuations $\propto(a^\dagger + a)$ of the cavity field lead to a decay rate $\gamma_\kappa = \kappa|\langle 0; gg|a|\psi\rangle|^2$ to the ground state [18,34]. The total decay rate is then given by $\gamma = \gamma_i + \gamma_\kappa$ with the intrinsic, nonradiative decay rate $\gamma_i$. Although the Purcell decay can be made small by operating the qubits in the dispersive regime $[\gamma_\kappa \approx (g/\Delta)^2\kappa]$ it cannot be fully avoided for transmon qubits. For the dark state, however, the matrix element $|\langle 0; gg|a|\psi_a\rangle|$ vanishes completely, since by symmetry $|\psi_a\rangle$ has no photon admixture. In other words, destructive interference of the photons emitted from either qubit leads to a suppression of the spontaneous emission process and the dark state is protected against Purcell decay.

In order to observe subradiant Purcell protection, we have detuned the qubits from the first harmonic mode by $\Delta/2\pi = -290$ MHz $\sim -2.5g$ into a regime where radiative losses dominate over intrinsic qubit losses ($\gamma_\kappa > \gamma_i$). At this frequency, the lifetime of the symmetric and antisymmetric state, as well as the decay rates of the individual qubits, have been measured. A delayed measurement pulse technique has been employed, where we apply a $\pi$ pulse resonant with the respective transition frequency and delay the time $\Delta t$ before applying the readout pulse. The lifetimes of single qubit excitations $T_{1,ge} = 401 \pm 16$ ns and $T_{1,eg} = 364 \pm 16$ ns at this frequency are comparable to the bright state lifetime of $T_{1,s} = 368 \pm 30$ ns. In contrast, the measured dark state lifetime $T_{1,a} = 751 \pm 13$ ns exceeds these values by a factor of 2—a clear signature of subradiance that demonstrates the decoupling of the antisymmetric state from the cavity environment and, as a consequence, its enhanced stability. The population decay versus time of both the bright and the dark state is plotted in Fig. 4(a).

The lifetime of the dark state is shown at different detunings in Fig. 4(b), along with the lifetimes of the bright state and the uncoupled single-qubit states. The effect of subradiant decay of the dark state is suppressed because of local dephasing acting on individual qubits. This process mixes symmetric and antisymmetric states by adding a random relative phase between the states $|ge\rangle$ and $|eg\rangle$. The rapidly decaying bright state contribution leads to a shorter effective lifetime of the dark state at small detunings. For the same reason, the superradiant decay rate of the bright state approaches the single-qubit Purcell-enhanced decay rate. This has been verified by numerical master equation simulations of the

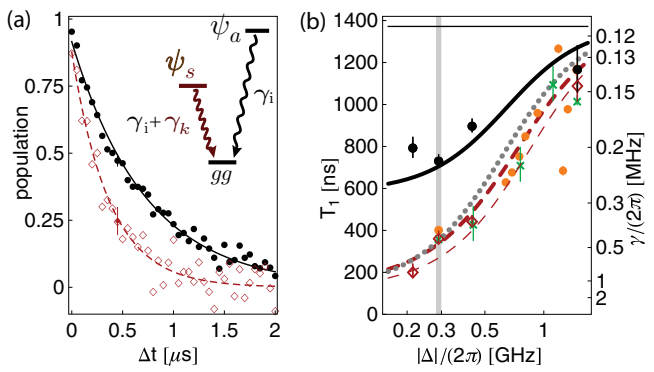


FIG. 4. (Color online) (a) Population of the antisymmetric dark ($\psi_a$, black dots) and the symmetric bright ($\psi_s$, red diamonds) state vs time at $\Delta/2\pi = -290$ MHz with exponential fits to the data. The inset shows the energy relaxation of $\psi_a$ and $\psi_s$. Only the symmetric state $\psi_s$ is affected by Purcell decay $\gamma_\kappa$. (b) Measured decay times of $\psi_s$ (red diamonds), $\psi_a$ (black dots) and uncoupled qubit states $|eg\rangle$ (orange points) and $|ge\rangle$ (green crosses) as a function of detuning $\Delta$. Exponential fits to numerically simulated populations are shown for $\psi_s$ (dashed lines), $\psi_a$ (solid lines), and $|eg\rangle$ (dotted line) including dephasing (thick lines) and without dephasing (thin lines). The vertical gray line indicates the frequency of the $T_1$ measurement in (a) and the spectroscopic measurements shown in Fig. 3.

dissipative dynamics for $\psi_a$ and $\psi_s$ using the pure dephasing rate of the individual qubits $\gamma_{2,\phi}/2\pi = 0.18$ MHz measured in independent Ramsey-fringe experiments.

In the context of quantum computation, the logical qubit formed by the ground and the dark state realizes a decoherence-free subspace [31,32], which is insensitive to cavity dissipation as well as to global dephasing acting simultaneously on both qubits. Note, however, that the subspace spanned by $|0; gg\rangle$, $|\psi_a\rangle$, and the doubly excited state $|0; ee\rangle$ forms a only weakly nonlinear qubit with anharmonicity $2J$, which sets a minimum time limit of $\sim 1/(2J)$ for gate operations without pulse optimization [43].

More generally, this local control technique may be used to excite highly entangled Dicke states belonging to different symmetry classes with a single microwave pulse conditioned on the choice of phases between individual drives. The possibility to address states of different symmetry classes of multiqubit systems can be exploited to encode information in collective qubit states. For readout, they can be transformed into entangled states in the computational basis by rapidly detuning the qubit transition frequencies out of qubit-qubit resonance.

In conclusion, we have demonstrated a method to populate dark states of a two-qubit system in circuit QED. The transitions to either dark or bright two-qubit states can be selected by adjusting the relative phase between individual qubit drives, thus changing the symmetry of the field and enforcing a symmetry-induced selection rule. With this technique we have demonstrated Purcell protection of the subradiant dark state against spontaneous emission. An extension to more qubits could provide further insight into the unitary and dissipative dynamics of multiparticle quantum states that can be directly prepared in the coupled qubit basis.

This work was supported by the Swiss National Science Foundation (SNF). S.F. acknowledges support by the Austrian Science Foundation (FWF). The authors thank A. Blais and J. Gambetta for valuable discussions.

[1] W. Ludwig and F. C., *Symmetries in Physics: Group Theory Applied to Physical Problems* (Springer, Berlin, 1988).
[2] R. H. Dicke, Phys. Rev. **93**, 99 (1954).
[3] M. Gross and S. Haroche, Phys. Rep. **93**, 301 (1982).
[4] H. Häffner *et al.*, Nature (London) **438**, 643 (2005).
[5] M. Eibl, N. Kiesel, M. Bourennane, C. Kurtsiefer, and H. Weinfurter, Phys. Rev. Lett. **92**, 077901 (2004).
[6] M. Neeley *et al.*, Nature (London) **467**, 570 (2010).
[7] O. Gühne, F. Bodoky, and M. Blaauboer, Phys. Rev. A **78**, 060301 (2008).
[8] W. Dür, G. Vidal, and J. I. Cirac, Phys. Rev. A **62**, 062314 (2000).
[9] H. J. Briegel and R. Raussendorf, Phys. Rev. Lett. **86**, 910 (2001).
[10] N. Sangouard, C. Simon, H. de Riedmatten, and N. Gisin, Rev. Mod. Phys. **83**, 33 (2011).
[11] D. A. Lidar and K. B. Whaley, in *Irreversible Quantum Dynamics*, edited by F. Benatti and R. Floreanini, Lecture Notes in Physics Vol. 622 (Springer, Berlin, 2003), pp. 83–120.
[12] A. Crubellier, S. Liberman, D. Pavolini, and P. Pillet, J. Phys. B **18**, 3811 (1985).
[13] A. Crubellier and D. Pavolini, J. Phys. B **19**, 2109 (1986); A. Crubellier, *ibid.* **20**, 971 (1987); A. Crubellier and D. Pavolini, *ibid.* **20**, 1451 (1987).
[14] D. Pavolini, A. Crubellier, P. Pillet, L. Cabaret, and S. Liberman, Phys. Rev. Lett. **54**, 1917 (1985).
[15] R. G. DeVoe and R. G. Brewer, Phys. Rev. Lett. **76**, 2049 (1996).
[16] A. Wallraff *et al.*, Nature (London) **431**, 162 (2004).
[17] A. Blais, R. S. Huang, A. Wallraff, S. M. Girvin, and R. J. Schoelkopf, Phys. Rev. A **69**, 062320 (2004).
[18] A. Houck *et al.*, Nature (London) **449**, 328 (2007).
[19] J. M. Fink *et al.*, Nature (London) **454**, 315 (2008).
[20] D. Bozyigit *et al.*, Nat. Phys. **7**, 154 (2011).
[21] J. M. Fink *et al.*, Phys. Rev. Lett. **103**, 083601 (2009).
[22] J. Majer *et al.*, Nature (London) **449**, 443 (2007).
[23] F. Altomare *et al.*, Phys. Rev. B **82**, 094510 (2010).
[24] S. Filipp *et al.*, Phys. Rev. A **83**, 063827 (2011).
[25] L. DiCarlo *et al.*, Nature (London) **460**, 240 (2009).
[26] H. Wang *et al.*, Phys. Rev. Lett. **106**, 060401 (2011).
[27] L. DiCarlo *et al.*, Nature (London) **467**, 574 (2010).
[28] E. M. Purcell, Phys. Rev. **69**, 681 (1946).
[29] A. A. Houck *et al.*, Phys. Rev. Lett. **101**, 080502 (2008).
[30] M. D. Reed *et al.*, Appl. Phys. Lett. **96**, 203110 (2010).
[31] J. M. Gambetta, A. A. Houck, and A. Blais, Phys. Rev. Lett. **106**, 030502 (2011).
[32] S. J. Srinivasan, A. J. Hoffman, J. M. Gambetta, and A. A. Houck, Phys. Rev. Lett. **106**, 083601 (2011).
[33] M. Tavis and F. W. Cummings, Phys. Rev. **170**, 379 (1968).
[34] J. Koch *et al.*, Phys. Rev. A **76**, 042319 (2007).
[35] P. J. Leek *et al.*, Phys. Rev. B **79**, 180511 (2009).
[36] A. Beige, S. F. Huelga, P. L. Knight, M. B. Plenio, and R. C. Thompson, J. Mod. Opt. **47**, 401 (2000).
[37] P. C. de Groot *et al.*, Nat. Phys. **6**, 763 (2010).
[38] J. M. Chow *et al.*, Phys. Rev. Lett. **107**, 080502 (2011).
[39] A. Wallraff *et al.*, Phys. Rev. Lett. **95**, 060501 (2005).
[40] R. Bianchetti *et al.*, Phys. Rev. A **80**, 043840 (2009).
[41] S. Filipp *et al.*, Phys. Rev. Lett. **102**, 200402 (2009).
[42] A. Abragam, *Principles of Nuclear Magnetism* (Oxford University Press, London, 1961).
[43] F. Motzoi, J. M. Gambetta, P. Rebentrost, and F. K. Wilhelm, Phys. Rev. Lett. **103**, 110501 (2009).